A transferable coarse-grained potential to study the structure of confined, supercritical Lennard-Jones fluids

T. Sanghi and N. R. Aluru[a)]
Department of Mechanical Science and Engineering, Beckman Institute for Advanced Science and Technology, University of Illinois at Urbana-Champaign, Urbana, Illinois 61801, USA

(Received 11 September 2009; accepted 16 December 2009; published online 27 January 2010)

In this paper, we develop a transferable coarse-grained interatomic potential to study the structure of simple (spherical and nonpolar) Lennard-Jones (LJ) fluids confined at supercritical temperatures. The potential is used in empirical potential based quasicontinuum theory, [A. V. Raghunathan *et al.*, J. Chem. Phys. **127**, 174701 (2007)] to study the structure of three simple LJ fluids (oxygen, methane, and argon) confined in slitlike geometries. The results obtained using the coarse-grained interatomic potential are found to be in good agreement with those predicted by equilibrium molecular dynamics simulations. © *2010 American Institute of Physics*. [doi:10.1063/1.3289722]

I. INTRODUCTION

Fluids confined between solid surfaces with separation ranging from micrometers to a few tens of nanometers are playing an increasingly important role in many scientific and engineering applications such as lab-on-a-chip, energy storage, water purification, and nanomanufacturing.[1–3] At nanometer scales, surface or interfacial behavior becomes important and confined fluid exhibits a wide range of phase behavior that is very different from the corresponding bulk state.[4] Owing to high inhomogeneity of confined fluids at these scales, continuum or classical theories, which assume a homogeneous variation in state variables, fail to predict the correct interfacial phenomena. Models based on statistical theory are used to study fluid confinement at nanometer scales. In statistical models, the macroscopic property of the fluid is obtained from the discrete particle information using a suitable averaging process. Atomistic molecular dynamics (MD) (Ref. 5) is one such simulation technique, which has been extensively used to study fluid flow at nanometer scales. While MD can accurately predict the interfacial phenomena, it requires significant computing resources and is practically limited to study phenomena on short length and time scales. This practical limitation of MD roots from the use of hard atomistic potentials, which limit the largest time step that can be used to perform a stable simulation. To overcome this limitation, the concept of *coarse-graining* (CG) is used. In CG, the hard atomistic interactions are replaced by softer interactions, which permit the use of a larger time step and enable the simulation of systems on bigger length and time scales. Coarse-grained potentials are constructed from the atomistic potentials either by averaging the molecular field over the rapidly fluctuating short time scale motions that are lesser relevant to the macroscale phenomena of interest,[6] or by parameterizing a predefined analytical form to reproduce some average thermodynamic or structural quantity obtained from atomistic simulations.[7] Although coarse-grained potentials allow the simulation of big and complex systems closer to experimental scales, they have some limitations. The coarse-grained potentials gain computational efficiency at the expense of the structural and chemical details of the system. During CG, the structural and chemical details of the system at scales smaller than the coarse-grained scale are completely lost. Also, most of the coarse-grained potentials perform well in the thermodynamic conditions of the reference atomistic system used to parameterize them and suffer from the loss of transferability.[8–10]

There are many complex fluids such as polymers whose macroscopic behavior is influenced by their dynamics on multiple length scales.[7] Also, many of the recent micro-electro-mechanical systems and nano-electro-mechanical systems applications use hybrid micronanofluidic devices where both the interfacial and the macroscopic behavior of the fluid are important. The use of classical theory to study such multiscale behavior can predict inaccurate results, while the use of MD simulation may not be possible because of computational limitations. Hence, in past few years a lot of effort has gone into developing *multiscale methods*,[11] which combine the atomic-scale and macroscale methods and attempt to provide a unified frame work to study fluid behavior across multiple length and time scales. Recently Raghunathan *et al.*[12] proposed an empirical potential based quasicontinuum theory (EQT) to obtain the equilibrium structure of confined fluids across multiple length scales. In EQT, one-dimensional steady-state Nernst–Planck equation[12,13]

$$\frac{d}{dx}\left(\frac{dc}{dx}+\frac{c}{RT}\frac{dU}{dx}\right)=0, \tag{1}$$

with boundary conditions

[a)]Author to whom correspondence should be addressed. Electronic mail: aluru@illinois.edu.

$$c(x=0)=0,$$

$$c(x=L)=0, \tag{2}$$

$$\frac{1}{L}\int_0^L c(x)dx = c_{\mathrm{av}},$$

is solved to obtain self-consistent potential and concentration profile of the confined fluid. Here c is the concentration, R is the gas constant, T is the temperature, and U is the total potential of the confined Lennard-Jones (LJ) fluid. L is the dimension of the confining geometry and c_{av} is the average concentration of the confined LJ fluid. A coarse-grained interatomic pair potential is used to compute the total potential U of the confined LJ fluid. This approach provides a means to capture the underlying atomistic physics in the interfacial region of the confined fluid without resorting to computationally expensive atomistic simulations. Also, unlike density-functional theory[14] and integral equation theory,[15] which involve calculation of computationally expensive free energy functional and pair functions and often require explicit approximations, EQT is a very simple and fast method to study fluid confinement at multiple length scales. In this paper we develop a transferable coarse-grained interatomic potential that is used in EQT to study the structure of confined, simple LJ fluids at supercritical temperatures. There are some important applications that involve the confinement of fluids near or above their critical temperature. One such application is the storage of high density methane (main constituent of natural gas) in micropores at near-ambient temperatures, well above its critical temperature (191 K).[16] Such storage methods are needed for efficient transportation of natural gas and fuel storage in vehicles.[17]

The remainder of the paper is organized as follows. In Sec. II, we first discuss the structural consistency of the coarse-grained interatomic pair potential used in EQT to study simple LJ fluids. Then we describe the development of the new coarse-grained potential, discuss the variation in its two CG parameters with the density and temperature of the supercritical LJ fluid and establish quantitative relations between them. The relations describe the variation in the CG parameters as a function of the bulk density and the temperature of the confined LJ fluid and provide transferability to the potential across different supercritical thermodynamic states. Details on EQT and various MD simulations performed to obtain the relations and to verify the results obtained from new coarse-grained potential are provided in Sec. III. In Sec. IV, we use the relations to study the effect of the density and temperature on the static structure of supercritical LJ oxygen confined between different width silicon slits. To check the transferability of the relations to different LJ fluids, they are used to study the equilibrium structure of supercritical LJ methane and argon confined in different width graphite slits. Results obtained using the relations are compared to those obtained from MD simulations. Finally, conclusions are presented in Sec. V.

II. COARSE-GRAINED INTERATOMIC PAIR POTENTIAL

A. Structural consistency

In EQT, Raghunathan *et al.*[12] used a coarse-grained interatomic pair potential, $u_{\mathrm{LJ}}^t(r)$, defined as

$$u_{\mathrm{LJ}}^t(r) = \begin{cases} 0 & r \le R_{\mathrm{crit}} \\ \left[2-\left(\frac{r}{R_{\mathrm{min}}}\right)^2\right]^4 \times \left[\frac{C_{12}^{\mathrm{ff}}}{R_{\mathrm{min}}^{12}} - \frac{C_6^{\mathrm{ff}}}{R_{\mathrm{min}}^6}\right] & R_{\mathrm{crit}} < r \le R_{\mathrm{min}} \\ \left[\frac{C_{12}^{\mathrm{ff}}}{r^{12}} - \frac{C_6^{\mathrm{ff}}}{r^6}\right] & r > R_{\mathrm{min}}, \end{cases} \tag{3}$$

to derive the total fluid-fluid interaction potential of confined simple LJ fluids. Here $C_{12}^{\mathrm{ff}}=4\epsilon_{\mathrm{ff}}\sigma_{\mathrm{ff}}^{12}$ and $C_6^{\mathrm{ff}}=4\epsilon_{\mathrm{ff}}\sigma_{\mathrm{ff}}^6$. ϵ_{ff} and σ_{ff} are the fluid-fluid LJ energy and distance parameters, respectively. R_{min} and R_{crit} are two CG parameters, which define the soft repulsive region and the zero potential core in the coarse-grained pair potential. The specific functional form of the soft-repulsive core is an ansatz and lacks any fundamental (microscopic) derivation. A coarse-grained potential can be used to obtain the equilibrium property of a system if the equilibrium probability density of a dynamical state of the system obtained from it is equal to that determined by the complete atomistic potential[9]

$$P_{\mathrm{CG}} = P_{\mathrm{atomistic}}. \tag{4}$$

Equation (4) defines the condition under which a coarse-grained potential for a system is structurally consistent with the complete atomistic potential for the same system. For a system in canonical (N,V,T) ensemble, the equilibrium probability density of a dynamical state as determined by the

soft repulsive core potential u_{LJ}^{soft} and the complete 12-6 LJ potential $u_{LJ}^{12\text{-}6}$ is

$$P_{LJ}^{soft} \propto \exp(-U_{LJ}^{soft}/K_BT),$$
$$P_{LJ}^{12\text{-}6} \propto \exp(-U_{LJ}^{12\text{-}6}/K_BT), \tag{5}$$

where U_{LJ}^{soft} and $U_{LJ}^{12\text{-}6}$ are the total potential energy of the given state obtained using u_{LJ}^{soft} and $u_{LJ}^{12\text{-}6}$, respectively. K_B is the Boltzmann constant and T is the absolute temperature of the system. Since the expression for the equilibrium probability density in Eq. (5) involves $\exp(-U/K_BT)$, all the states for which U is positive and larger than few K_BT have almost zero equilibrium probability and make negligible contribution to the equilibrium properties of the system. The CG strategy of replacing the hard repulsive form of the 12-6 LJ potential with a softer and finite form in the region $r<\sigma_{ff}$, thus does not significantly affect the equilibrium probability distribution of the system. These coarse-grained LJ potentials are made structurally consistent by choosing a suitable softer repulsive form and adjusting the CG parameters such that the equilibrium probability distribution of the system obtained from them is equal to that obtained from complete 12-6 LJ potential. Such coarse-grained LJ potentials have been used by Mezei[18] to calculate the excess free energy of the dense LJ fluids. Soft interatomic potentials have also been used successfully in conventional molecular simulations and in dissipative particle dynamics[19] to study the equilibrium properties of soft materials.

Raghunathan *et al.*[12] used u_{LJ}^{t} given by Eq. (3) to develop a quasicontinuum potential model for confined simple LJ fluids. In quasicontinuum model, the total potential $U(r)$ is computed by using the continuum approximation on the discrete summation expression for the total potential obtained from molecular representation, i.e.,

$$U(r) = \sum_{i=1}^{N_f} u_{LJ}^{12\text{-}6}(|r-r_i|), \tag{6}$$

$$\approx \int_{\Omega} u_{LJ}^{12\text{-}6}(|r-r'|)\rho_f(r')d\Omega, \tag{7}$$

$$\approx \int_{\Omega} u_{LJ}^{t}(|r-r'|)\rho_f(r')d\Omega, \tag{8}$$

where N_f is the number of fluid atoms surrounding the fluid atom at position r, r_i is the location of fluid atom i, and ρ_f is the density of fluid atoms in the volume element $d\Omega$. The reason for using a truncated soft core repulsive potential u_{LJ}^{t} instead of the complete 12-6 LJ potential to obtain the total potential of a confined fluid ($\rho_f(r') \neq$ const) is to avoid numerical singularities that occur while computing the integral given by Eq. (7) in the region $0<|r-r'|<\sigma_{ff}$. For confined fluids, in the void region ($\rho_f(r') \simeq 0$) next to the walls, the integrand $u_{LJ}^{12\text{-}6}(|r-r'|)\rho_f(r')$ in Eq. (7) should $\to 0$. However, because of the very strong repulsive nature of the 12-6 LJ potential in the region $|r-r'|<\sigma_{ff}$, this product can diverge even when $\rho_f(r') \to 0 (u_{LJ}^{12\text{-}6}(\sim 10^{16}) \times \rho_f(\sim 10^{-6}))$. Also, in the highly inhomogeneous interfacial region, where $\rho_f(r')$ is high and $|r-r'|<\sigma_{ff}$, the product $u_{LJ}^{12\text{-}6}(|r-r'|)\rho_f(r')$ could become very large and give rise to significant numerical errors, while computing the integral over the entire domain. Hence, to avoid the divergence in the void region and minimize the numerical errors, the potential is truncated in a small region around the point of singularity ($0 \le r \le R_{crit}$) and made softer in the region $R_{crit} \le r \le R_{min}$. To investigate the effect of this CG strategy, we use u_{LJ}^{t} to compute the total potential U_{LJ}^{t} at a point r due to a homogeneous ($\rho_f(r')$ =const) semi-infinite fluid volume of thickness Δ. The final expression for $U_{LJ}^{t}(r)$ obtained from Eq. (8) is given by

$$U_{LJ}^{t}(r) = \rho\Delta \begin{cases} f(R_{crit}) + g(R_{min}) & r \le R_{crit} \\ f(r) + g(R_{min}) & R_{crit} < r \le R_{min} \\ g(r) & r > R_{min}, \end{cases} \tag{9}$$

where functions f and g are defined as

$$f(x) = \frac{\pi R_{min}^2}{5}\left[\frac{C_{12}^{ff}}{R_{min}^{12}} - \frac{C_6^{ff}}{R_{min}^{6}}\right]\left[\left\{2 - \left(\frac{x}{R_{min}}\right)^2\right\}^5 - 1\right],$$
$$g(x) = \frac{\pi C_{12}^{ff}}{5}\left(\frac{1}{x^{10}}\right) - \frac{\pi C_6^{ff}}{2}\left(\frac{1}{x^4}\right). \tag{10}$$

Figure 1(a) shows the comparison of $U_{LJ}^{t}(r)$ and $U_{LJ}^{12\text{-}6}(r)$. $U_{LJ}^{12\text{-}6}(r)$ is the total potential obtained by using the complete 12-6 LJ potential [Eq. (7)] and is given by

$$U_{LJ}^{12\text{-}6}(r) = \rho\Delta g(r). \tag{11}$$

It can be observed that U_{LJ}^{t} is exactly same as $U_{LJ}^{12\text{-}6}$ until $r=R_{min}$, has softer repulsive interaction between R_{crit} and R_{min} and becomes constant for $r \le R_{crit}$. The strength of the repulsive interaction can be controlled by changing the CG parameters R_{min} and R_{crit}, and the potential could be easily parameterized to reproduce the desired equilibrium property of the homogeneous fluids. For confined fluids, the potential is parameterized by adjusting the CG parameters R_{min} and R_{crit} to match the variation in the total interaction potential U_{Tot}^{CG} obtained using continuum approximation [Eq. (8)] with the total potential U_{Tot}^{MD} obtained from representative molecular system. The total interaction potential of the confined simple LJ fluid is the summation of the wall-fluid and the fluid-fluid interaction potentials. The wall-fluid potential $U_{wall\text{-}fluid}$ is calculated by modeling the wall as semi-infinite continuum of uniformly distributed atoms and using the complete 12-6 LJ wall-fluid potential in Eq. (7). This approach was originally discussed by Steele.[20,21] We discuss two different wall-fluid potential models in Sec. III. Fluid-fluid interaction potential $U_{fluid\text{-}fluid}^{CG}$ is calculated from Eq. (8).[12] The parametrization procedure is summarized in Algorithm I. Once the coarse-grained potential is parameterized

for a particular thermodynamic state, it is used in EQT (Ref. 12) to obtain the concentration profile of the confined fluid in different width channels. It is important to note that the parametrization procedure explicitly involves $\rho(r)$ and $U_{\mathrm{Tot}}^{\mathrm{MD}}$ from the reference molecular level system. Thus, the CG parameters obtained for one thermodynamic state are in general not transferable to a different thermodynamic state.[10]

Algorithm I Parametrization of the coarse-grained potential.

1: Input: $\rho(r)$ and total interaction potential ($U_{\mathrm{Tot}}^{\mathrm{MD}}$) from representative molecular level system.

2: Compute wall-fluid interaction potential, $U_{\text{wall-fluid}}$, using Eq. (16) provided in Sec. III.

3: Take initial guess for R_{min} and R_{crit}.

4: Compute fluid-fluid interaction potential, $U_{\text{fluid-fluid}}^{\mathrm{CG}}$, using $\rho(r)$ and u_{LJ}^{t} in Eq. (8).

5: Calculate $U_{\mathrm{Tot}}^{\mathrm{CG}}=U_{\text{wall-fluid}}+U_{\text{fluid-fluid}}^{\mathrm{CG}}$.

6: Obtain R_{min} and R_{crit} by solving the nonlinear equation $U_{\mathrm{Tot}}^{\mathrm{CG}}(R_{\mathrm{min}},R_{\mathrm{crit}})-U_{\mathrm{Tot}}^{\mathrm{MD}}=0$.

B. Transferable potential: Relationship between coarse-graining parameters and density and temperature of the fluid

To develop a transferable potential, we explore the variation in the CG parameters with the independent thermodynamic variables of the fluid. In supercritical state, for a one component fluid, both temperature and density can be independently changed without altering the state of the system. To understand the connection of the CG parameters with the density and temperature of the fluid, we use a second order polynomial functional form to model softer interactions and define a new coarse-grained interatomic pair potential, $u_{\mathrm{LJ}}^{\mathrm{CG}}(r)$, as

$$u_{\mathrm{LJ}}^{\mathrm{CG}}(r)=\begin{cases}0 & r\le R_{\mathrm{crit}}\\ a_0+a_1r+a_2r^2 & R_{\mathrm{crit}}<r\le R_{\mathrm{min}}\\ \left[\dfrac{C_{12}^{\mathrm{ff}}}{r^{12}}-\dfrac{C_6^{\mathrm{ff}}}{r^6}\right] & R_{\mathrm{min}}<r\le R_{\mathrm{cut}},\end{cases}\tag{12}$$

where C_{12}^{ff}, C_6^{ff}, ϵ_{ff}, σ_{ff}, R_{min}, and R_{crit} have their usual meaning as defined above. a_0, a_1, and a_2 are the coefficients of the polynomial form, and are calculated to ensure the continuity of the softer potential and its first and second derivatives with the 12-6 LJ potential at R_{min}. R_{cut} is a cutoff distance beyond which pairwise LJ interaction is assumed to be zero. One important difference in this new coarse-grained potential is that it ensures the continuity of the force (first derivative of the potential) at R_{min}, which was not enforced in the original coarse-grained potential u_{LJ}^{t}. To test the performance of this new potential, it is parameterized to predict the concentration and potential profiles of LJ oxygen confined between different width silicon slits at 300 K. The density of the confined fluid is $\rho^{*}=1.08$. Here $\rho^{*}(=\rho\sigma_{\mathrm{ff}}^{3})$ is the nondimensional number density. This value corresponds to a bulk density of $\rho=32$ atoms/nm^3. The parametrization is done by using $u_{\mathrm{LJ}}^{\mathrm{CG}}$ in place of u_{LJ}^{t} in Algorithm I. $\rho(r)$ and $U_{\mathrm{Tot}}^{\mathrm{MD}}$ are obtained from MD simulation of LJ oxygen confined in a $11\sigma_{\mathrm{ff}}$ wide nanochannel. There is no restriction on the size of the MD system to be used to parameterize the coarse-grained potential. It could be any reasonable size system in which both the wall-fluid and the fluid-fluid potential contribute to the structural inhomogeneity. Very small size systems ($L\sim 2\sigma_{\mathrm{ff}},3\sigma_{\mathrm{ff}}$) should be avoided because in such systems the wall-fluid interactions are typically the only dominant interactions that cause structural inhomogeneity. Equation (16) with $c_{\mathrm{wall}}=80$ atoms/nm^3 is used to compute the wall-fluid interaction potential. The total fluid-fluid interaction potential $U_{\text{fluid-fluid}}^{\mathrm{CG}}$ at a point x inside the channel is given by

$$\begin{aligned}U_{\text{fluid-fluid}}^{\mathrm{CG}}(x)=&\int_{x}^{x+R_{\mathrm{crit}}}[f(R_{\mathrm{crit}})+g(R_{\mathrm{min}})]\rho(x')dx'+\int_{x+R_{\mathrm{crit}}}^{x+R_{\mathrm{min}}}[f(x')+g(R_{\mathrm{min}})]\rho(x')dx'+\int_{x+R_{\mathrm{min}}}^{x+R_{\mathrm{cut}}}[g(x')]\rho(x')dx'\\&+\int_{x-R_{\mathrm{crit}}}^{x}[f(R_{\mathrm{crit}})+g(R_{\mathrm{min}})]\rho(x')dx'+\int_{x-R_{\mathrm{min}}}^{x-R_{\mathrm{crit}}}[f(x')+g(R_{\mathrm{min}})]\rho(x')dx'+\int_{x-R_{\mathrm{cut}}}^{x-R_{\mathrm{min}}}[g(x')]\rho(x')dx',\end{aligned}\tag{13}$$

where for $u_{\mathrm{LJ}}^{\mathrm{CG}}$, functions f and g are defined as

$$\begin{aligned}f(x)&=2\pi\left[\frac{a_0}{2}(R_{\mathrm{min}}^2-x^2)+\frac{a_1}{3}(R_{\mathrm{min}}^3-x^3)+\frac{a_2}{4}(R_{\mathrm{min}}^4-x^4)\right],\\g(x)&=\frac{\pi C_{12}^{\mathrm{ff}}}{5}\left(\frac{1}{x^{10}}-\frac{1}{R_{\mathrm{cut}}^{10}}\right)-\frac{\pi C_6^{\mathrm{ff}}}{2}\left(\frac{1}{x^4}-\frac{1}{R_{\mathrm{cut}}^4}\right),\end{aligned}\tag{14}$$

$R_{\mathrm{min}}=1.078\sigma_{\mathrm{ff}}$ and $R_{\mathrm{crit}}=0.34\sigma_{\mathrm{ff}}$ give a good match between the total interaction potential $U_{\mathrm{Tot}}^{\mathrm{CG}}$ obtained using the continuum approximation and $U_{\mathrm{Tot}}^{\mathrm{MD}}$ obtained from MD simulation. These values are different from those obtained for u_{LJ}^{t} ($R_{\mathrm{min}}=0.939\sigma_{\mathrm{ff}}$ and $R_{\mathrm{crit}}=0.29\sigma_{\mathrm{ff}}$) (Ref. 12) under the same thermodynamic conditions. Figure 2 shows the variation in concentration profiles of LJ oxygen across $20\sigma_{\mathrm{ff}}$ and $7\sigma_{\mathrm{ff}}$ wide nanochannels obtained using $u_{\mathrm{LJ}}^{t}(r)$ and $u_{\mathrm{LJ}}^{\mathrm{CG}}(r)$ in EQT. It can be observed that the concentration and potential profiles are in good agreement with each other and with the results obtained from MD simulations.

To find the variation in the coarse-grained parameters with the change in density and temperature of the confined LJ fluid, MD simulations of the LJ oxygen confined between $11\sigma_{\mathrm{ff}}$ wide silicon slit are carried out at several density and temperature values ($\rho^{*}=1.08$, 0.764, and 0.48; T=200, 300,

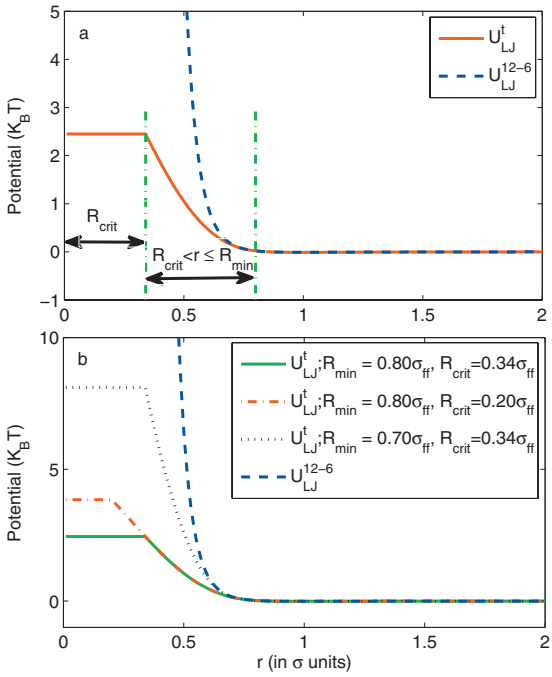

FIG. 1. (a) Comparison of the total potential U^t_{LJ} and U^{12-6}_{LJ} of a homogeneous fluid obtained using u^t_{LJ}, and u^{12-6}_{LJ}, respectively. (b) Variation in U^t_{LJ} with R_{crit} and R_{min}.

and 400 K). $\rho^*=0.764$ and 0.48 correspond to a bulk density of $\rho=25$ atoms/nm^3 and $\rho=15$ atoms/nm^3, respectively. All these temperature values are greater than the critical temperature of the bulk oxygen (155 K).[16] Statistical theories for confined fluids predict that the critical temperature of a fluid under confinement lies substantially below its critical temperature in the bulk state.[22] Hence, the systems considered above are representative of a supercritical LJ fluid confined in a silicon slit. The details on the molecular model and simulation parameters are given in Sec. III. Two interesting observations are made while parameterizing the new coarse-grained potential u^{CG}_{LJ} for these systems at aforementioned density and temperature values. (1) It is found that once the potential is parameterized for a given density and temperature, for a change in thermodynamic state that involves varying the density of the fluid at a fixed temperature, the potential could be reparameterized by adjusting the parameter R_{crit} alone, keeping the parameter R_{min} fixed for the given temperature. (2) Similarly, for a change in the thermodynamic state that involves varying the temperature of the fluid at a fixed density, the potential could be reparameterized by adjusting the parameter R_{min} alone, keeping the parameter R_{crit} fixed for the given density. These observations connect the change in the CG parameters R_{crit} and R_{min} with the change in the density and temperature of the confined fluid. Figure 3 shows the variation in nondimensional CG parameters, $R^*_{crit}(=R_{crit}/\sigma_{ff})$ and $R^*_{min}(=R_{min}/\sigma_{ff})$, as a function of nondimensional density, ρ^*, and nondimensional LJ energy parameter, ϵ^* $(=\epsilon_{ff}/K_BT)$, respectively. It can be seen that the parameter R_{crit} decreases linearly with increase in density. This trend can be understood from Fig. 1(b). It can be observed that soft-repulsive potential exists until $r=R_{crit}$, below which it becomes constant in the region $r\leq R_{crit}$. A smaller R_{crit} value corresponds to a larger extent of the soft-repulsive interactions. At higher densities, excluded volume effects dominate and the structure of simple liquids is mainly determined by the repulsive interactions.[23–25] Hence, when density increases, R_{crit} decreases to increase the strength and extent of the repulsive interactions, required to obtain the correct equilibrium structure at higher densities. Like R_{crit}, R_{min} also decreases linearly with increase in the temperature of the confined fluid. This observation can be understood from the role temperature plays in determining the equilibrium structure of the confined fluid. Increase in temperature induces thermal fluctuations and increases the probability of the fluid atoms to move around the potential minimum. R_{min} is the distance until which the exact 12-6 LJ potential is used in the coarse-grained potential and its value always lies in the interval $R_{crit}<R_{min}<2^{1/6}\sigma_{ff}$; $2^{1/6}\sigma_{ff}$ is the distance at which the minimum of LJ potential occurs. Hence, when temperature increases, R_{min} decreases to increase the extent of the actual 12-6 LJ potential around energy minima, required to capture fluctuations at higher temperatures. For u^{CG}_{LJ}, R^*_{crit}, and R^*_{min} are related to ρ^* and ϵ^* as

$$R^*_{crit} = 0.7361 - 0.3652\rho^*,$$
$$R^*_{min} = 1.0311 + 0.1745\epsilon^*. \quad (15)$$

These relations are obtained from first order least squares fit

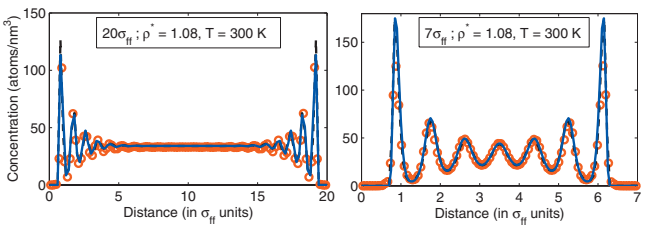

FIG. 2. Comparison of the concentration profiles of supercritical LJ oxygen ($\rho^*=1.08$ and T=300 K) across $20\sigma_{ff}$ (left) and $7\sigma_{ff}$ (right) wide silicon slits. The dashed and the solid lines are the results obtained using u^t_{LJ} and u^{CG}_{LJ}, respectively. Open circle is the MD data.

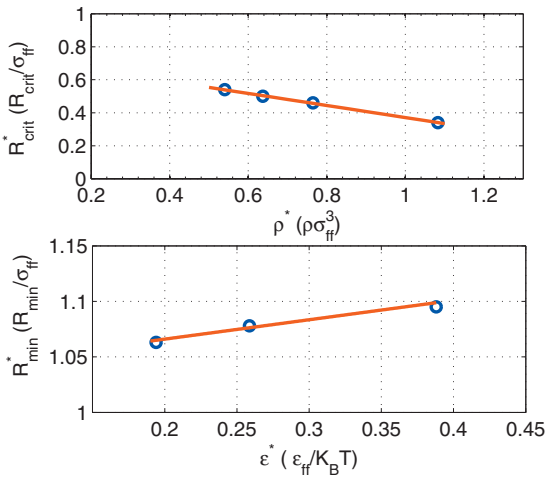

FIG. 3. Variation in the nondimensional CG parameters R^*_{crit} (top) and R^*_{min} (bottom) of u^{CG}_{LJ} with nondimensional density, ρ^*, and energy, ϵ^*, respectively. The circle denotes the value obtained for confined LJ oxygen (system I) using MD data of a $11\sigma_{ff}$ wide channel. Solid line represents the first order least squares fit [Eq. (15)].

of the R_{crit} and R_{min} values (denoted by circle in Fig. 3) obtained from the parametrization of the coarse-grained potential at various density and temperature values considered above and correspond to ρ^* and ϵ^* in the range $0.48 \leq \rho^* \leq 1.08$ and $0.19 \leq \epsilon^* \leq 0.388$, respectively.

III. SIMULATION DETAILS

Relations given by Eq. (15) are used to parameterize the new coarse-grained potential u_{LJ}^{CG} for confined simple LJ fluids in different supercritical states. Parameterized potential is used in EQT to investigate the fluid confinement in three systems. System I consists of LJ oxygen molecules confined between silicon slit and system II and III contain spherical methane and argon molecules, respectively, confined between different width graphite slits. Two different wall models are used to compute the total wall-fluid potential in EQT. In the first model, the spacing between the lattice planes is neglected and walls are modeled as flat infinite continuum of atoms. For such a wall, the total wall-fluid potential at a point x normal to the structureless wall is given by the 9-3 potential[21]

$$U_{\text{wall-fluid}}(x) = 2\pi c_{\text{wall}}\left[\frac{C_{12}^{\text{wf}}}{90}\left(\frac{1}{x^9}\right) - \frac{C_6^{\text{wf}}}{12}\left(\frac{1}{x^3}\right)\right], \tag{16}$$

where $C_{12}^{\text{wf}}=4\epsilon_{\text{wf}}\sigma_{\text{wf}}^{12}$ and $C_6^{\text{wf}}=4\epsilon_{\text{wf}}\sigma_{\text{wf}}^6$. ϵ_{wf} and σ_{wf} are the wall-fluid LJ energy and distance parameters, respectively. c_{wall} is the number density of the wall atoms. In the second model, walls are treated as stacked planes of atoms separated by distance Δx, spacing between the planes. The total wall-fluid potential at a point x from such a wall is given by the 10-4-3 potential[26]

$$U_{\text{wall-fluid}}(x) = 2\pi\epsilon_{\text{wf}}\sigma_{\text{wf}}^2\Delta x c_{\text{wall}} \times\left[\frac{2}{5}\left(\frac{\sigma_{\text{ff}}^{10}}{x^{10}}\right) - \left(\frac{\sigma_{\text{ff}}^4}{x^4}\right) - \left(\frac{\sigma_{\text{ff}}^4}{\Delta x(0.61+x)^3}\right)\right]. \tag{17}$$

Here ϵ_{wf}, σ_{wf}, and c_{wall} have their usual meaning as defined above. The "10" and "4" terms represent the repulsive and attractive interactions of the fluid molecule with the first plane of atoms, and the "3" term results from the summation of the attraction term over the remaining layers of the solid. Continuum 9-3 potential given by Eq. (16) is used to model silicon-oxygen interactions in system I. Graphite-methane and graphite-argon interactions in system II and III are modeled using 10-4-3 potential given in Eq. (17).

Concentration and potential profiles obtained from EQT are compared to those obtained from equilibrium MD simulations. We have used the same molecular model as used by Raghunathan *et al.*[12] for system I. For systems II and III, molecular wall consists of four graphene layers, with an interlayer spacing of 0.335 nm. The number density of the carbon atoms in the graphite is 114 atoms/nm^3. The dimensions of the wall in y and z directions are 4.550 and 4.331 nm, respectively. The LJ force field parameters used in the MD simulation are listed in Table I.[12,26,27] A time step of 2 fs was used to simulate the system. LJ cutoff distance was set to 1.38 nm. The temperature of the fluid was maintained using a Nosé–Hoover thermostat,[28] with a time constant of 0.5 ps. The *NVT* MD simulations were performed using GROMACS.[29]

TABLE I. Parameters for the LJ potential.

Interaction	C_6 (kJ nm^6 mol^{-1})	C_{12} (kJ nm^{12} mol^{-1})	σ (nm)
O–O	$0.261\,87\times10^{-2}$	$0.263\,07\times10^{-5}$	0.3170
O–Si	$0.623\,37\times10^{-2}$	$0.769\,29\times10^{-5}$	0.3277
Si–Si	$0.147\,38\times10^{-1}$	$0.221\,91\times10^{-4}$	0.3385
CH_4–CH_4	$0.151\,02\times10^{-1}$	$0.463\,41\times10^{-4}$	0.3812
CH_4–C	$0.470\,88\times10^{-2}$	$0.103\,53\times10^{-4}$	0.3606
C–C	$0.143\,96\times10^{-2}$	$0.222\,39\times10^{-5}$	0.3400
Ar–Ar	$0.621\,94\times10^{-2}$	$0.969\,29\times10^{-5}$	0.3405
Ar–C	$0.288\,71\times10^{-2}$	$0.432\,40\times10^{-5}$	0.3383
C–C	$0.133\,98\times10^{-2}$	$0.192\,79\times10^{-5}$	0.3360

IV. RESULTS

A. System I: Supercritical oxygen confined between planar silicon walls

To test the accuracy of the relations obtained for R_{crit} and R_{min}, they are used to predict the concentration profile of supercritical LJ oxygen confined between planar silicon walls at $\rho^*=0.64$ and T=300 K. This density value corresponds to a bulk density of $\rho=20$ atoms/nm^3. For this density value, Eq. (15) gives $R_{crit}=0.50\sigma_{ff}$. $R_{min}=1.078\sigma_{ff}$ is used at T=300 K. Figure 4 shows the comparison of concentration profiles across $4\sigma_{ff}$ and $5\sigma_{ff}$ wide nanochannels obtained from EQT and the MD simulations. It can be observed that except for a slight mismatch in the first peak next to each wall, the concentration profiles obtained using the R_{crit} and R_{min} values obtained from Eq. (15) match quite well with those from MD simulations. The difference in the first peak comes mainly from the error in the wall-fluid potential closer to the wall. This error could be reduced by using more advanced models,[20,21] which take into account both the structure and the spacing of the lattice planes and provide a more realistic description for the solid-fluid interactions. To compare the effect of density on the fluid density distribution at a fixed temperature, concentration profiles at two different density values ($\rho^*=1.08, 0.48$) are also plotted in Fig. 4. $R_{crit}=0.34\sigma_{ff}$ and $0.54\sigma_{ff}$ is used for $\rho^*=1.08$ and 0.48, respectively. It can be observed that the number of layers inside the nanochannels changes with density and increasing the density at a fixed temperature enhances the effect of the surface on the fluid density distribution. These observations can be explained by comparing the distance of the first peak from the wall and the total number of peaks in the central region of the channel. For both the channels, at all density values, the first peak always lies at approximately $0.88\sigma_{ff}$ distance away from the wall. For $5\sigma_{ff}$ wide channel, at $\rho^*=1.08$, there are three fluid layers in the central region ($\sim 3\sigma_{ff}$) of the channel, while the number of layers in the same length of region is two at $\rho^*=0.64$ and 0.48. Similarly, for $4\sigma_{ff}$ wide channel, there are two layers in the central region ($\sim 2\sigma_{ff}$) at $\rho^*=1.08$, but only one layer for $\rho^*=0.64$

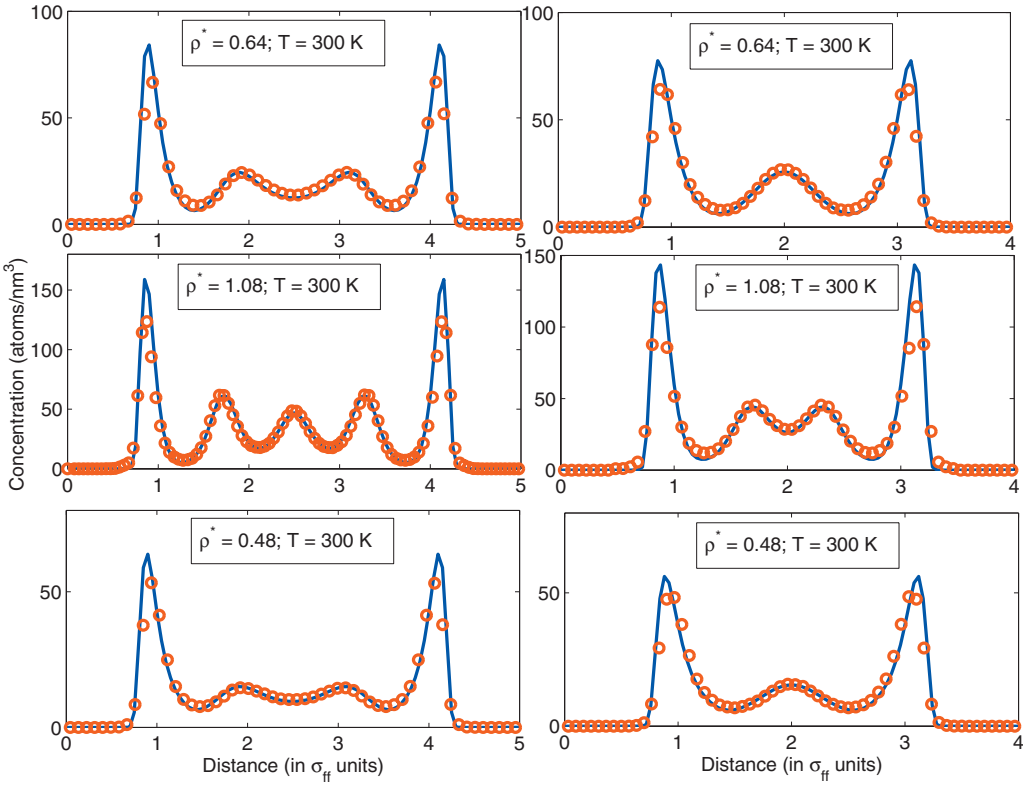

FIG. 4. Comparison of the concentration profiles of supercritical LJ oxygen inside $5\sigma_{ff}$ (left) and $4\sigma_{ff}$ (right) wide silicon slits at $\rho^*=0.64$, 1.08, and 0.48 and T=300 K. Solid line represents the result from EQT and circles are the MD results.

and 0.48. At lower densities, although there is sufficient space in the central region to accommodate one more fluid layer, it cannot be achieved without leaving voids (more repulsive force) and only occurs at higher density. Figure 5 shows the comparison of concentration profile across $7\sigma_{ff}$ and $11\sigma_{ff}$ wide nanochannels at three different temperatures (T=200, 300, and 400 K). To study the effect of temperature on the fluid structure, the density is kept constant ($\rho^*=1.08$) in all the three systems. For this density, $R_{crit}=0.34\sigma_{ff}$ is used. $R_{min}=1.095\sigma_{ff}$, $1.078\sigma_{ff}$, and $1.063\sigma_{ff}$ is used for T=200, 300, and 400 K, respectively. Again, except for the first peak, there is a good match between the profiles obtained from EQT and MD simulations. It can be observed that the inhomogeneity decreases with increase in temperature. This observation can be understood from the fact that increase in temperature induces thermal fluctuations in the fluid structure. Thermal fluctuations increase the probability of an atom to move around its minimum energy position and weaken the layering induced by the surface.

B. System II: Supercritical methane confined between planar graphite walls

To test the transferability of the relations obtained for R_{crit} and R_{min} to a different LJ fluid, we use them to obtain the concentration and potential profiles of supercritical LJ methane confined between planar graphite walls at 296 K. The density of the confined fluid is $\rho^*=1.0$. It corresponds to a bulk density of $\rho=18$ atoms/nm^3. For this density and temperature value, from Eq. (15), we get $R_{crit}=0.37\sigma_{ff}$ and $R_{min}=1.118\sigma_{ff}$. Figure 6 shows the concentration profile of LJ methane confined inside different width graphite slits. It can be observed that the new potential captures the correct atomistic physics near the interface and predicts both the *interfacial* layering near the wall and the *bulk* behavior at the center of $15\sigma_{ff}$ channel. For smaller channels there is no bulk region and confinement makes the fluid density inhomogeneous across the total width of the channel. Again, except for a slight deviation in the first peak, the results obtained from EQT using u_{LJ}^{CG} match quite well with those obtained from MD simulations. It is interesting to note that there is inconsistency in the total number of peaks in the concentration profile of smaller channels. The number of peaks in $7\sigma_{ff}$ and $6\sigma_{ff}$ wide nanochannels are 7 and 6, respectively, while $5\sigma_{ff}$, $4\sigma_{ff}$, and $3\sigma_{ff}$ wide nanochannels have 4, 3, and 2 peaks, respectively. This inconsistency happens because of an overlap between the wall-fluid potentials from the opposite walls in smaller dimension channels. Figure 7 shows the wall-fluid and fluid-fluid interaction potential across $5\sigma_{ff}$, $4\sigma_{ff}$, and $3\sigma_{ff}$ wide nanochannels. It can be observed that for smaller dimension channels, wall-fluid potential plays the dominant role in determining the equilibrium structure of the confined fluid. For $3\sigma_{ff}$ channel, there is a big overlap of the wall-fluid potential from the opposite walls and the two peaks in the concentration profile result from the two minima in the wall-fluid interaction potential. Fluid-fluid interaction potential at the given density does not contribute to any additional layer and there is no third layer in the central region of the channel. Similarly, for $4\sigma_{ff}$, and $5\sigma_{ff}$ wide nanochannels, due to a substantial overlap in the wall-fluid potential, it makes favorable contribution (negative potential) to the minima in the fluid-fluid potential, which enhances the layering in the first

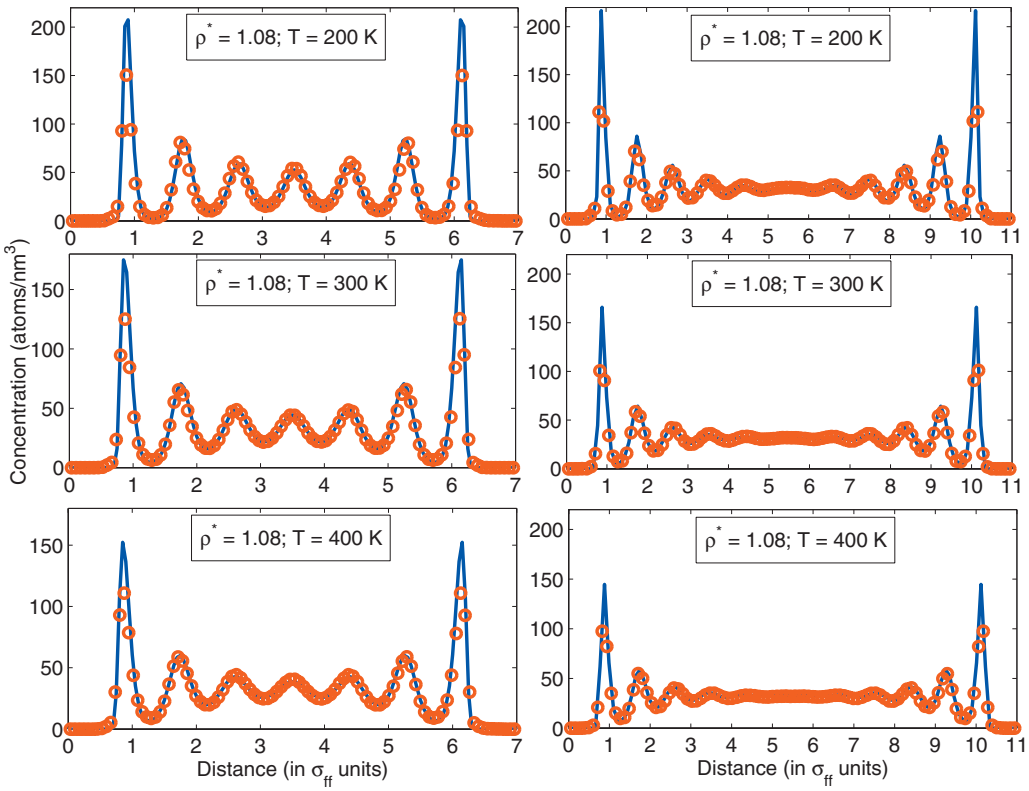

FIG. 5. Comparison of the concentration profiles of supercritical LJ oxygen inside $7\sigma_{ff}$ (left) and $11\sigma_{ff}$ (right) wide silicon slits at $\rho^*=1.08$ and T=200, 300, and 400 K. Solid line represents the results from EQT and circles are the MD results.

two layers next to the wall and results in reduction in one complete layer in the central region of the nanochannels. As the channel dimension increases, the overlap in the wall-fluid potential decreases, and it only contributes to the first layer next to each wall and rest of the layers come from the inhomogeneity in the fluid-fluid interaction potential. The CG parameters obtained from Eq. (15) are able to predict this structural inconsistency quite accurately. The relations are

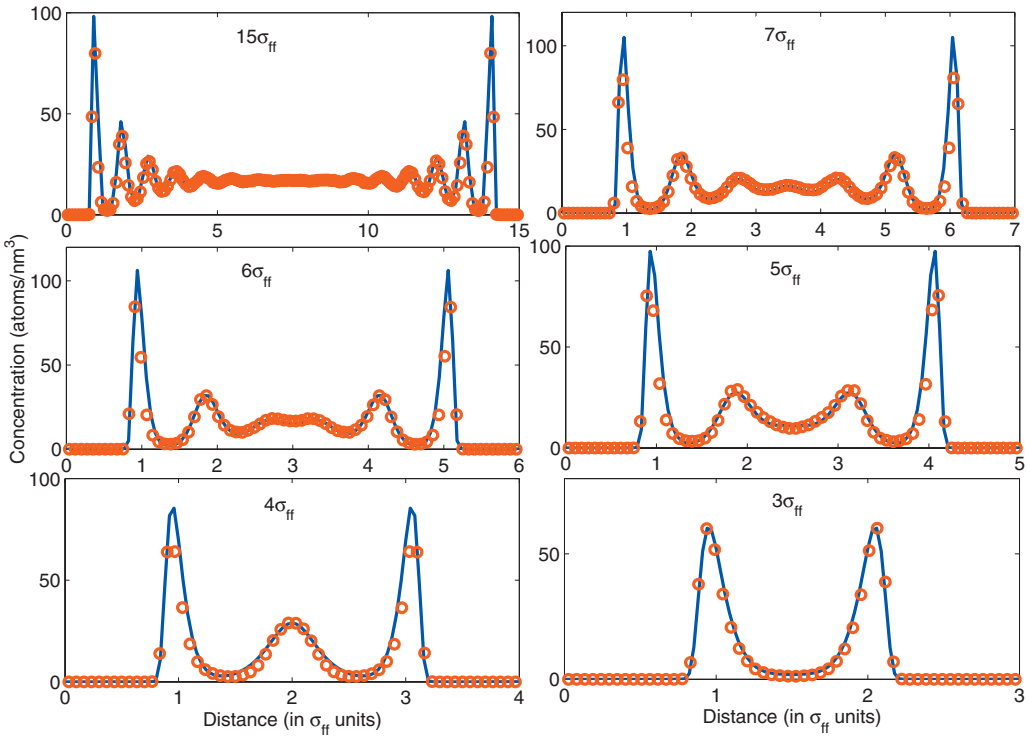

FIG. 6. Comparison of the concentration profiles of supercritical LJ methane inside $15\sigma_{ff}$, $7\sigma_{ff}$, $6\sigma_{ff}$, $5\sigma_{ff}$, $4\sigma_{ff}$, and $3\sigma_{ff}$ wide graphite slits. Solid line represents the results from EQT and circles are the MD results.

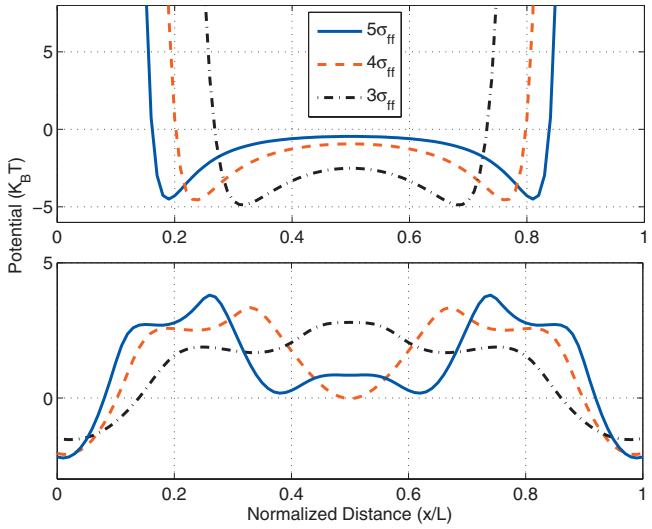

FIG. 7. Wall-fluid (top) and fluid-fluid potential (bottom) of confined LJ methane ($\rho^*=1.00$ and T=296 K) across $5\sigma_{ff}$, $4\sigma_{ff}$, and $3\sigma_{ff}$ wide graphite slits. L is the width of the channel and x is the perpendicular distance from the wall.

also used to obtain the density profile at $\rho^*=1.0$ and T=400 K. Equation (15) gives $R_{min}=1.09\sigma_{ff}$ for T=400 K. $R_{crit}=0.37\sigma_{ff}$ is used for $\rho^*=1.0$. The density profiles inside different width nanochannels obtained using these parameters in u_{LJ}^{CG} compare reasonably well with those obtained from MD simulations, thus establishing the transferability of the relations to confined supercritical LJ methane. To further check the accuracy of the relations for this system, the R_{crit} and R_{min} values obtained from Eq. (15) are compared to those obtained from Algorithm I. For $\rho^*=1.0$ and T=296 K, the values obtained from Algorithm I are $R_{crit}=0.375\sigma_{ff}$ and $R_{min}=1.120\sigma_{ff}$. These values are in good agreement with the values obtained above ($R_{crit}=0.37\sigma_{ff}$ and $R_{min}=1.118\sigma_{ff}$) from Eq. (15).

C. System III: Supercritical argon confined between planar graphite walls

The relations are also used to study the equilibrium structure of supercritical LJ argon confined between planar graphite walls at 300 K, well above its critical temperature (151 K).[16] The density of the confined fluid is $\rho^*=0.95$. This density value corresponds to a bulk density of $\rho=24$ atoms/nm^3. For this density and temperature value, Eq. (15) predicts $R_{crit}=0.389\sigma_{ff}$ and $R_{min}=1.10\sigma_{ff}$. Figure 8 shows the concentration profile of LJ argon confined between different width graphite slits. It can be observed that the density profiles obtained using u_{LJ}^{CG} with R_{crit} and R_{min} values obtained from Eq. (15) in EQT match well with those obtained from MD simulations. Like confined methane molecules, there is an inconsistency in the total number of peaks observed in smaller width nanochannels. The total number of peaks in $11\sigma_{ff}$ wide nanochannel is 11, while $6\sigma_{ff}$, $5\sigma_{ff}$, $4\sigma_{ff}$, and $3\sigma_{ff}$ wide channels have 5, 4, 3, and 2 peaks, respectively. This inconsistency can again be explained from the dominant behavior of the wall-fluid potential in smaller dimension channels. Again, to check the accuracy of the relations, the R_{crit} and R_{min} values obtained from Eq. (15) are compared to those obtained from Algorithm I. For $\rho^*=0.95$ and T=300 K, Algorithm I predicts $R_{crit}=0.385\sigma_{ff}$ and $R_{min}=1.105\sigma_{ff}$, which are in close agreement with the values obtained above ($R_{crit}=0.389\sigma_{ff}$ and $R_{min}=1.10\sigma_{ff}$) for this system.

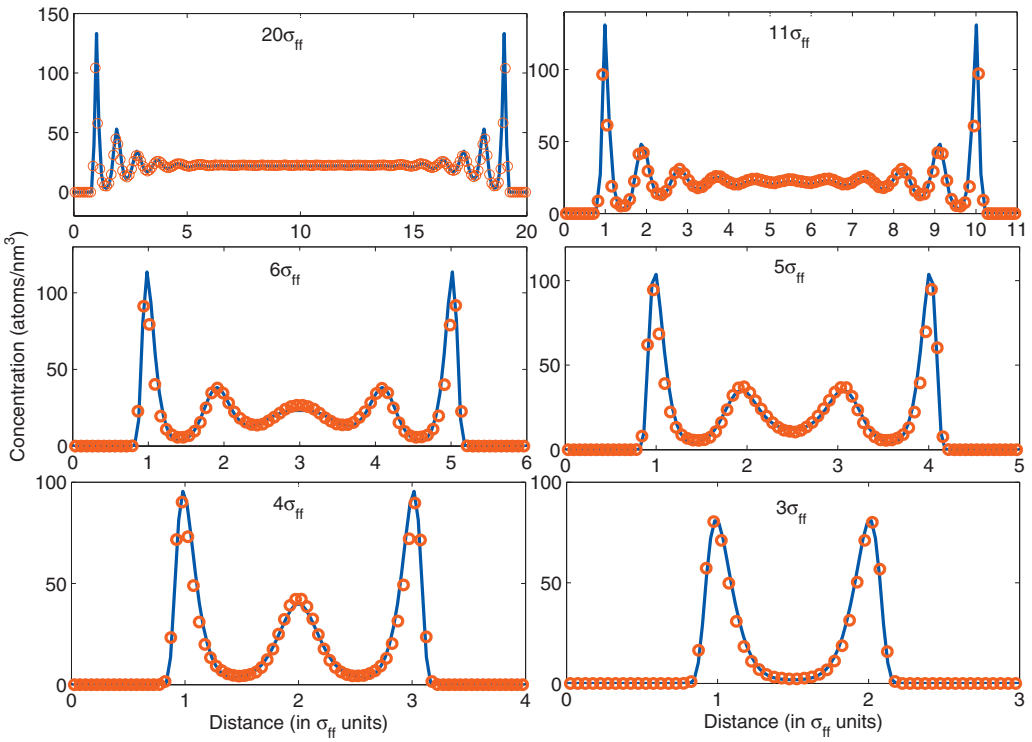

FIG. 8. Comparison of the concentration profiles of supercritical LJ argon inside $20\sigma_{ff}$, $11\sigma_{ff}$, $6\sigma_{ff}$, $5\sigma_{ff}$, $4\sigma_{ff}$, and $3\sigma_{ff}$ wide graphite slits. Solid line represents the results from EQT and circles are the MD results.

V. CONCLUSIONS

In this work, a transferable coarse-grained interatomic potential is developed to study the structure of confined, simple LJ fluids at supercritical temperatures. Two relations are obtained, which describe the change in the CG parameters as a function of bulk density and temperature of the confined LJ fluid and provide transferability to the coarse-grained potential. The relations can be used to obtain the numerical value of the CG parameters for any combination of bulk density and temperature of the confined supercritical LJ fluid, and are used to study the effect of density and temperature on the static structure of supercritical LJ oxygen confined in different width silicon slits. The concentration and potential profiles obtained using the relations match well with those obtained from MD simulations. To test the applicability of the relations to different LJ fluid-slit systems, they are used to study the equilibrium structure of high density ($\rho^* \sim 1$) supercritical LJ methane and argon confined at near ambient ($T \sim 300$ K) temperatures. For both the fluids, the concentration profiles obtained using the CG parameters given by the relations match quite well with those obtained from MD simulations. Thus, relations provide transferability to the coarse-grained potential and save a significant computational effort, which otherwise would have been required to parameterize the potential in different supercritical states and for different LJ fluid-slit systems. The relations are found to work reasonably well for ρ^* and ϵ^* in the range $0.48 \leq \rho^* \leq 1.08$ and $0.19 \leq \epsilon^* \leq 0.50$, respectively. More simulations could be performed to further improve the relations and extend them beyond the range considered in this paper. With these transferable relations, the new coarse-grained potential can be parameterized without requiring any MD simulation, and can be directly used in EQT to study the equilibrium structure of confined supercritical LJ fluids in a computationally efficient manner.

ACKNOWLEDGMENTS

This work was supported by NSF under Grant No. 0120978 (Water CAMPWS, UIUC), Grant No. 0328162 (nano-CEMMS, UIUC), Grant Nos. 0625421, 0810294, 0852657, and 0915718. T.S. thanks A. V. Raghunathan for helpful discussions.

[1] T. Thorsen, S. J. Maerkl, and S. R. Quake, Science **298**, 580 (2002).
[2] J. L. Perry and S. G. Kandlikar, Microfluid. Nanofluid. **2**, 185 (2006).
[3] B. Van der Bruggen, C. Vandecasteele, T. V. Gestel, W. Doyen, and R. Leysen, Environ. Prog. **22**, 46 (2004).
[4] R. Evans, J. Phys.: Condens. Matter **2**, 8989 (1990).
[5] D. Frenkel and B. Smith, *Understanding Molecular Simulation* (Academic, New York, 2001).
[6] B. M. Forrest and U. W. Suter, J. Chem. Phys. **102**, 7256 (1995).
[7] F. Müller-Plathe, ChemPhysChem **3**, 754 (2002).
[8] P. Carbone, H. A. K. Varaneh, X. Chen, and F. Müller-Plathe, J. Chem. Phys. **128**, 064904 (2008).
[9] W. G. Noid, J.-W. Chu, G. S. Ayton, V. Krishna, S. Izvekov, G. A. Voth, A. Das, and H. C. Andersen, J. Chem. Phys. **128**, 244114 (2008).
[10] A. A. Louis, J. Phys.: Condens. Matter **14**, 9187 (2002).
[11] S. Attinger and P. Koumoutsakos, *Multiscale Modelling and Simulation* (Springer, New York, 2004).
[12] A. V. Raghunathan, J. H. Park, and N. R. Aluru, J. Chem. Phys. **127**, 174701 (2007).
[13] T. Teorell, Prog. Biophys. Biophys. Chem. **3**, 305 (1953).
[14] R. Evans, *Density Functionals in the Theory of Nonuniform Fluids* (Dekker, New York, 1992).
[15] D. Henderson, *Integral Equation Theories for Inhomogeneous Fluids* (Dekker, New York, 1992).
[16] J. Vrabec, J. Stoll, and H. Hasse, J. Phys. Chem. B **105**, 12126 (2001).
[17] Z. Tan and K. E. Gubbins, J. Phys. Chem. **94**, 6061 (1990).
[18] M. Mezei, Mol. Simul. **2**, 201 (1989).
[19] R. D. Groot and P. B. Warren, J. Chem. Phys. **107**, 4423 (1997).
[20] W. A. Steele, *Interaction of Gases with Solid Surfaces* (Pergamon, New York, 1974).
[21] W. A. Steele, Surf. Sci. **36**, 317 (1973).
[22] K. Morishige and M. Shikimi, J. Chem. Phys. **108**, 7821 (1998).
[23] J.-P. Hansen and I. R. McDonald, *Theory of Simple Liquids* (Academic, New York, 2006).
[24] J. D. Weeks, D. Chandler, and H. C. Andersen, J. Chem. Phys. **54**, 5237 (1971).
[25] D. Chandler, J. D. Weeks, and H. C. Andersen, Science **220**, 787 (1983).
[26] D. Nicholson, Carbon **36**, 1511 (1998).
[27] B. Coasne, S. K. Jain, and K. E. Gubbins, Eur. Phys. J. Spec. Top. **141**, 121 (2007).
[28] S. Nosé, J. Chem. Phys. **81**, 511 (1984).
[29] E. Lindahl, B. Hess, and D. van der Spoel, J. Mol. Model. **7**, 306 (2001).